# Accepted Manuscript

Optical and theoretical investigation of Indian yellow (euxanthic acid and euxanthone)

Charlotte Martin de Fonjaudran, Angela Acocella, Gianluca Accorsi, Diego Tamburini, Giovanni Verri, Amarilli Rava, Samuel Whittaker, Francesco Zerbetto, David Saunders
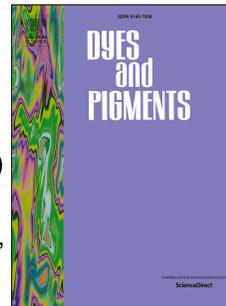
Please cite this article as: Martin de Fonjaudran C, Acocella A, Accorsi G, Tamburini D, Verri G, Rava A, Whittaker S, Zerbetto F, Saunders D, Optical and theoretical investigation of Indian yellow (euxanthic acid and euxanthone), *Dyes and Pigments* (2017), doi: 10.1016/j.dyepig.2017.05.034.
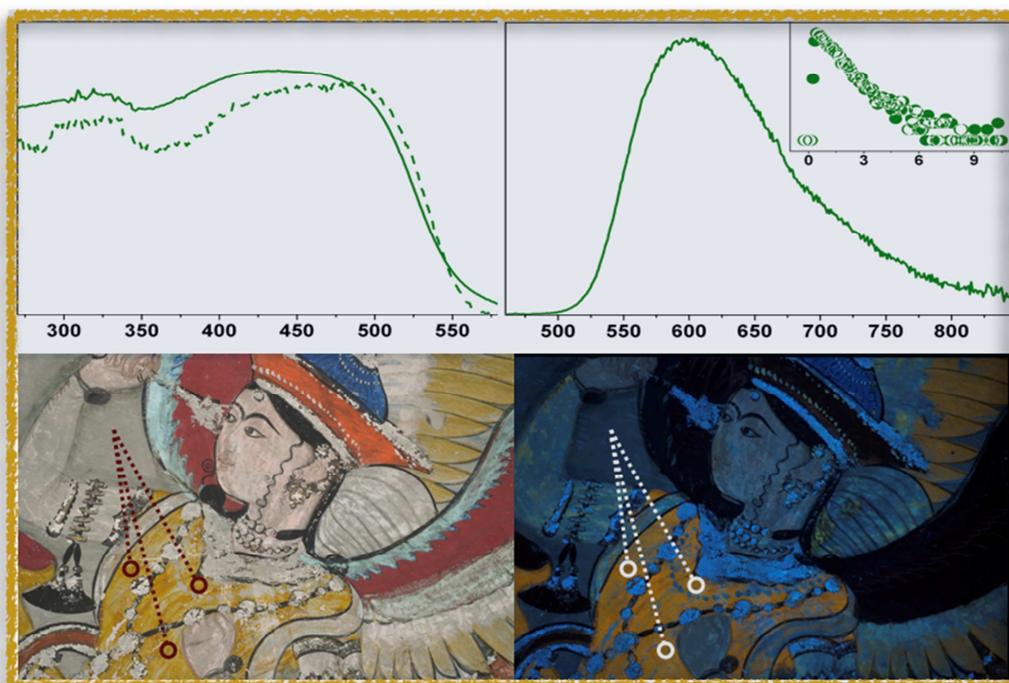
Textual abstract:

The optical properties and DFT calculations of Indian Yellow are here described and correlated to its chemical composition.

1 **OPTICAL AND THEORETICAL INVESTIGATION OF INDIAN YELLOW (EUXANTHIC**

2 **ACID AND EUXANTHONE).**

3 Charlotte Martin de Fonjaudran,[a] Angela Acocella,[b*] Gianluca Accorsi,[c*] Diego Tamburini, [d]

4 Giovanni Verri,[a*] Amarilli Rava, [a] Samuel Whittaker, [a] Francesco Zerbetto [b] and David Saunders [d]

[a] *The Courtauld Institute of Art, Somerset House, Strand, WC2R 0RN, London, UK, E-mail:*

6 *giovanni.verri@courtauld.ac.uk, Tel: +44 (0)29 84 21 64; charlotte.martinde@courtauld.ac.uk,*

7 *amarilli.rava@courtauld.ac.uk, samuelwhittaker@gmail.com*

8 [b] *Dipartimento di Chimica "G.Ciamician", Università di Bologna, Via F. Selmi 2, 40126, Bologna,*

9 *Italy. E-mail: angela.acocella3@unibo.it, francesco.zerbetto@unibo.it*

10 [c] *CNR NANOTEC - Institute of Nanotechnology c/o Campus Ecotekne, University of Salento; Via*

11 *Monteroni - 73100 Lecce, Italy. E-mail: gianluca.accorsi@nanotec.cnr.it, Tel: +39 0832 319813*

12 [d] *Department of Scientific Research, The British Museum, Great Russell Street, London WC1B 3DG,*

13 *UK, E-mail: DTamburini@britishmuseum.org, DSaunders@britishmuseum.org*

14 **ABSTRACT**

15 The optical properties (photophysics and imaging) of Indian yellow were investigated both in solid

16 state and in aqueous solution and correlated with its chemical composition. The analyses were

17 corroborated by a theoretical study carried out on the different xanthone derivatives that comprise

18 the pigment under investigation, both as isolated molecules and in a polar (protic) solvent, to help

19 the assignment of the excited states involved in the photo-induced process. Knowledge of its

20 relatively high photoluminescence quantum yield (PLQY 0.6%), excitation and emission spectra

21 and lifetime decays enhances the potential for reliable identification using non-invasive photo-

22 induced luminescence imaging techniques. New insights into the chemical composition of the

23 pigment, such as the identification of a sulphonate derivative of euxanthone, and its extensive

24 occurrence on a 17th-century Indian wall painting are also reported for the first time in this study.

25 *Keywords: Indian yellow; Photoluminescence spectroscopy; Time-dependent Density Functional*

26 *Theory Calculation; Photoluminescence imaging; Indian wall painting*

1. INTRODUCTION

Indian yellow, a historic pigment produced in India until the end of the 19th / beginning of the 20th century, is characterised by its luminous yellow-orange colour and noticeable photoluminescence properties. The main colorant is based on the crystalline mixture of the magnesium and calcium salts of euxanthic acid, EA [1]. One of the most frequently cited accounts of its production method states that the pigment derives from the urine of cows fed solely on mango leaves, a process which allegedly caused their premature death and led to a ban on production [1-3]. Early chemical studies showed that euxanthone ($C_{13}H_8O_4$), or its precursor present in mango leaves, can combine with glucuronic acid metabolised by mammals such as cows or rabbits and be excreted as a salt of EA ($C_{19}H_{16}O_{10}$) [4, 5]. However, some scholars have questioned this production process and the reasons behind its discontinuation [6-9].

Indian yellow has been identified on several miniature paintings dated between the 16th and 19th centuries that are attributed to the Mughal and Rajput schools [1, 10-12]. It was also used by artists in Europe and the United States [13-17]. However, its extensive occurrence on a monumental painting is reported for the first time in this study, following analyses of the yellow pigments used in the wall paintings decorating the Badal Mahal within Garh Palace in Bundi (Rajasthan, India). The painted scheme, dated to 1620–30, is one of the most significant within the palace complex. Depictions of courtly life, unfolding on the walls, are among the earliest and finest in Rajasthan. [18]. Other subject matters include a *Ragmala* series as well as scenes of Hindu mythology on the ceiling.

Light microscopy, XRD, SEM-EDX and FTIR were most commonly employed at the end of the 20th century to identify Indian yellow on works of art [1, 12, 13, 17]. More recently, other micro-destructive techniques such as NMR, HPLC-DAD [19] and LC-ESI/MS [15] have been applied to the identification of this unusual pigment. Non-invasive analytical techniques are now favoured for the preliminary study of artefacts and portable XRF and FTIR are more routinely used in the cultural heritage field [20-23]. While such techniques can be combined with imaging [20, 24], the

2

53 instruments commonly employed in museums or in the field provide only point analyses, thus

54 limiting the information available on the distribution of pigments of interest over large areas. Photo-

55 induced luminescence (PL) imaging, using ultraviolet (UV) excitation and recording visible

56 emission with a photographic camera, has been used since the late 1980s to highlight the possible

57 presence of Indian yellow [1, 13, 25, 26]. However, several other organic colorants commonly

58 encountered on Asian paintings also show comparable fluorescence when excited with UV

59 radiation [27], thus limiting possible differentiation between original materials. Nonetheless, PL

60 imaging using digital cameras offers an invaluable and affordable tool, which has been successfully

61 applied to the characterisation of several pigments such as Egyptian blue, Han blue, manganese

62 blue and cadmium-based pigments [28-30]. PL spectroscopy presents a necessary complementary

63 technique to corroborate the results and inform PL imaging protocols. The luminescence properties

64 of several pigments, such as lithopone [31], zinc oxide [32], zinc sulphide [33], manganese blue

65 [29], Egyptian blue [34, 35] and cadmium-based pigments [36-38], have been investigated in recent

66 years using both steady-state and time-resolved PL spectroscopy. However, the only published

67 study on Indian yellow presents a limited view of its excitation and emission profiles, with data

68 uncorrected for instrument response [1].

69   A complete understanding of the photophysical properties of Indian yellow is required for

70 correct interpretation of results obtained with PL spectroscopy and imaging techniques. In this

71 study, the organic chemical components of two samples, from a reference archive at the National

72 Gallery, London (NG) and from the wall painting in Bundi (B64), were identified with HPLC-ESI-

73 Q-ToF. The optical properties of the Indian yellow reference sample, that is the absorbance (total

74 reflection), excitation and emission profiles, as well as the lifetime decay were characterised both in

75 the solid state (as powder) and in solution (water) and compared to the emission profile and lifetime

76 decay of the wall painting sample. PL imaging, using a customised DSLR camera, xenon flashes

77 and bandpass filters, aimed to characterise visible and infrared (IR) emission following UV

78 excitation.

79   In an attempt to resolve the optical structure of the pigment, a theoretical study at the DFT

80   level of theory was conducted on euxanthic acid (EA), 4-sulphonate euxantohne (SE) and

81   euxanthone (E), both in the gas phase and in water, to support the experimental component. DFT

82   calculations were also run for 1-hydroxy-7-methyl-xanthone (OH-CH$_3$-X) and xanthone (X), to

83   investigate the role of substituents on the UV/Vis spectra and to make a comparative analysis with

84   previous results on X [39-42]. The chemical structures of all the compounds investigated are shown

85   in Scheme1.
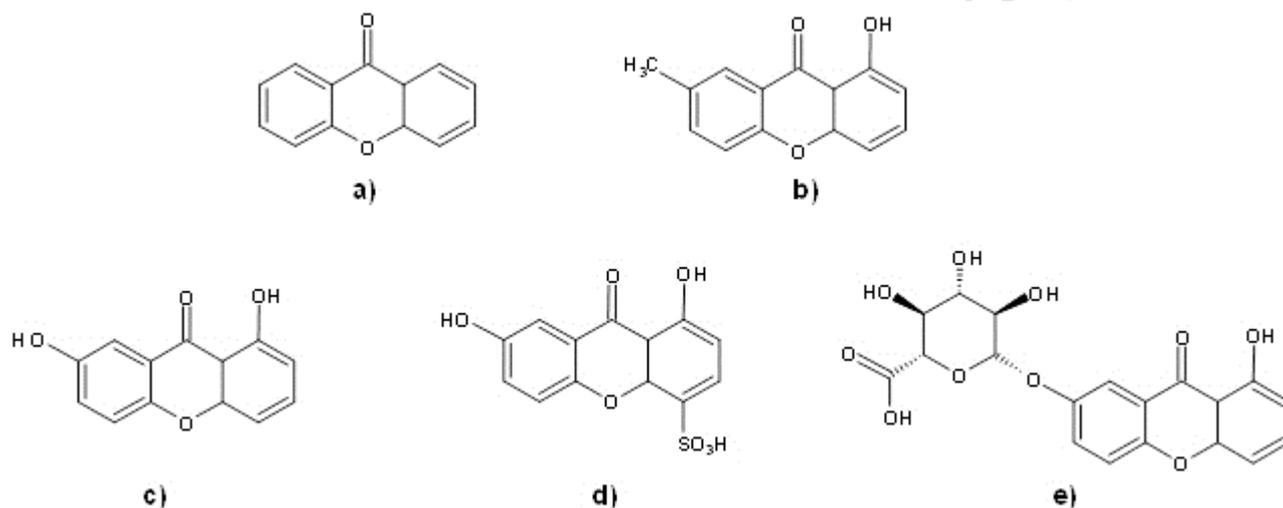
86

87   **Scheme 1**. Chemical structure of a) xanthone (X), b) 1-hydroxy-7-methyl-xanthone (OH-CH$_3$-X),

88   c) euxanthone (E), d) 4-sulphonate-euxanthone (SE), and e) euxanthic acid (EA).

89

90   **2. EXPERIMENTAL**

91   **2.1 Indian yellow samples**

92   A powdered sample (NG) of historic reference material was provided by the National

93   Gallery, London. The wall painting sample (B64) was taken from a yellow paint layer on the south

94   wall of the Badhal Mahal, in Garh Palace, Bundi (Rajasthan, India). An image of the area where the

95   sample was taken and a detail of a cross-section are shown in Figure 1. Yellow paint layers are

96   extensively used for the geometrical and floral patterns unfolding on the walls and for the garments

97   of Krishna and the *gopis* engaged in a circular dance depicted on the ceiling.

4

98

Fig. 1 Location of sample B64 on the south wall of the Badal Mahal, Garh Palace, Bundi (Rajasthan, India). Inset: cross-section illustrating the stratigraphy of the paint layer composed of a white ground and a single yellow layer.

2.2 HPLC-DAD-ESI-Q-ToF

For analysis with High-Performance Liquid Chromatography coupled to Electrospray Ionisation and Quadropole Time-of-Flight, samples (*c.*100 µg) were admixed with 200 µL DMSO and heated at 80°C for 10 minutes. After centrifugation, the supernatant was transferred into another vial. The residue was admixed with 200 µL of methanol/acetone/water/0.5M oxalic acid 30:30:40:1 (v/v/v/v) and heated at 80°C for 15 minutes. The solution was evaporated under N_2 and reconstituted using 200 µL of $MeOH/H_2O$ 1:1 (v/v). The DMSO extract was combined with the oxalic acid extract and the solution was centrifuged for 10 minutes. The supernatant was transferred to a fresh 250 µL insert and 5-10 µL of the solution were injected into the HPLC system.

Analyses were carried out using a 1260 Infinity HPLC (Agilent Technologies), coupled to a Quadrupole-Time of Flight tandem mass spectrometer 6530 Infinity Q-ToF detector (Agilent Technologies) by a Jet Stream ESI interface (Agilent Technologies). The HPLC conditions were: Zorbax Extend-C18 column (2.1 mm × 50 mm, 1.8 µm particle size); 0.4 mL/min flow rate; 5 µL injection volume for MS experiments and 10 µL for MSMS experiments; 40°C

5

117　column temperature. Separation was achieved using a gradient of water with 0.1% formic acid

118　(eluent A) and acetonitrile with 0.1% formic acid (eluent B). The elution gradient was

119　programmed as follows: initial conditions 95% A, followed by a linear gradient to 100% B in

120　10 min, then held for 2 min. Re-equilibration time for each analysis was 10 min. The ESI

121　operating conditions were: drying gas (N_2, purity >98%): 350°C and 10 L/min; capillary

122　voltage 4.0 kV; nebulizer gas 276 kPa; sheath gas (N_2, purity >98%): 375°C and 11 L/min.

123　　　High resolution MS and MS/MS spectra were acquired in negative mode in the range

124　100-1700 m/z. The fragmentor was kept at 150 V, nozzle voltage 1000 V, skimmer 65 V,

125　octapole RF 750 V. For the MS/MS experiments, different voltages in the collision cell were

126　tested for Collision Induced Dissociation (CID), in order to maximise the information obtained

127　from the fragmentation. The collision gas was nitrogen (purity 99.999%). The data were

128　collected by targeted MS/MS acquisition with an MS scan rate of 1.0 spectra/sec and a MS/MS

129　scan rate of 1.0 spectra/sec. MassHunter® Workstation Software was used to carry out mass

130　spectrometer control, data acquisition, and data analysis

131　**2.3 Optical measurements**

132　　　The photophysical properties of Indian yellow, in both solid state and solution, were

133　investigated using a Perkin-Elmer Lambda 1050 UV-Vis-NIR equipped with an integrating sphere

134　(total reflection measurements). The emission and excitation spectra were recorded by an

135　Edinburgh FLS980 spectrometer equipped with a Peltier-cooled Hamamatsu R928 photomultiplier

136　tube (185-850 nm) and a xenon lamp (450 W) as light source. To determine the luminescence

137　quantum yield, the method proposed by De Mello *et al*. was followed [43]. The emission lifetimes

138　in the pico- to nanosecond timescale were measured using a single photon counting system

139　(Edinburgh FLS980 spectrometer) with a 1 MHz laser diode as excitation source coupled with a

140　Hamamatsu MCP R3809U-50, time resolution 20 ps, as detector.

141

142

6

2.4 Imaging

The PL luminescence of the paintings in the Badal Mahal was recorded using a customised Nikon D7000. The removal of the camera's internal IR blocking filter and replacement with a quartz filter, allows detection of emission from *c*.350-1100 nm. The excitation source consisted of two Quantum Instruments T5dR xenon flashes, equipped with Xnite 330C and Xnite CC1 bandpass filters (*c*.280-400 nm). The camera was fitted with a cut-on Schott KV418 ultraviolet-blocking filter (50% transmission at 418 nm) and an IDAS-UIBAR bandpass filter (*c*.400-700 nm) to record emission in the visible, and Xnite 715 filter (50% transmission at 715 nm) to record emission in the IR. A white board covering the entire field of view, a Gretag-Macbeth ColorChecker chart, and a set of lambertian reflectance standards (Spectralon® 99, 75, 50 and 2%) were inserted in all images to allow for post-capture processing and correction (light distribution, colour correction, removal of ambient stray light) using Nip2 software and following the protocol described in Dyers *et al.* [44].

2.5 Calculations

In order to select the most suitable functional to gain meaningful results, the ground state geometries of EA, SE and E were optimised in the gas phase with the Gaussian09 suite of programs [45] at different hybrid and long-range corrected DFT functionals (namely, B3LYP [46], pure PBE [47], PBE0 [48], HSE06 [49], CAM-B3LYP [50] and LC-wPBE [51]) at the TZVP basis set level of theory. This set of functionals was selected to encompass a wide number of parameters, such as, corrections (or not) for dispersion effects and global or range-separated hybrids. Relative vertical electronic excitations, (transitions) dipole moments and oscillator strengths were obtained, at the corresponding level of theory, with the Time Dependent Density Function Theory (TDDFT) [52], generally used to reproduce the UV/Vis spectra of most organic [53-56] and inorganic dyes [57, 58]. The energetic positions of the triplet states are here analogously investigated, since X and some of its analogues are largely used as triplet sensitizers.

7

169 To mimic the solvent environment, the CPCM polarisable conductor model implemented in

170 Gaussian09 [59, 60] with the Pauling cavity set [61] and combined with a TD-DFT scheme, has

171 proven to be appropriate to reproduce the experimental absorption/excitation spectra for EA, SE

172 and E in water, with a high level of accuracy. B3LYP/CPCM and TDDFT(B3LYP)/CPCM

173 calculations were carried out to obtain optimised geometries and vertical excitation energies of EA,

174 E and SE in water.

175 Additional TDDFT calculations at the same level of theory were run on OH-CH$_3$-X and X

176 molecules to obtain complete information about the effect that substituents on the main xanthone

177 structure have on the position of the absorption bands, and to compare results with previous

178 literature data available on X.

179

180 **3. RESULTS AND DISCUSSION**

181 **3.1 Chemical composition**

182 HPLC-ESI-Q-ToF analysis revealed that both samples were composed of euxanthone (E)

183 and euxanthic acid (EA), in agreement with the literature [15]. Nevertheless, a third component was

184 also detected, and identified as a sulphonate derivative of euxanthone (SE), ($C_{13}H_8O_7S$). The

185 identification of SE was based on the high resolution mass data and the MSMS fragmentation

186 spectrum. The mass obtained for the molecular ion was $[M]^- = 306.9922$ uma and it showed a -1.21

187 ppm difference from the calculated mass (calculated $[M]^- = 306.9918$ uma). The MSMS spectrum

188 showed a main fragmentation peak at *m/z* 227.0353, corresponding to euxanthone (ppm difference -

189 1.39) and derived from the loss of a SO_3 moiety. Although the exact position of the sulphonate

190 group was not ascertained, we hypothesise that the C_4 position is that undergoing reaction, based on

191 the structure of other natural sulphonated xanthones [62].

192 Semi-quantitative calculations were performed to evaluate differences in the distribution of E,

193 EA and SE between sample S64 and the reference sample (NG). Chromatographic area ratios were

194 calculated by considering the sum of the chromatographic areas of E, EA and SE as 100%. Using

8

195 this method the percentage areas were EA = 77.4 ± 0.8%, SE = 14.7 ± 0.6% and E = 7.9 ± 0.2% for

196 sample NG and EA = 65.4 ± 0.4%, SE = 28.9 ± 0.4% and E = 5.6 ± 0.1% for sample S64 (standard

197 deviation refer to triplicate measurements). It is important to underline that these values do not

198 necessarily correspond to the actual percentage contents of the three components in the samples,

199 because the ionisation yield of each compound may vary. Nevertheless, the results can be used to

200 compare the samples and a higher relative abundance of SE was observed for sample B64 compared

201 to NG.

202 Although Indian yellow has been characterised by LC-MS analysis previously [15], this work

203 presents the first identification of euxanthone-4-sulphonate. Its presence in the wall painting sample

204 (B64) makes it unlikely to result from a synthetic production process and would rather point

205 towards a natural occurrence. In fact, sulphonation and glucoronidation are two competitive

206 mechanisms in the metabolism of mammals, especially for phenolic molecules, and sulphonation

207 usually occurs in parallel to glucoronidation, but to a lesser extent [63, 64]. This could be taken as

208 further evidence that a metabolic pathway is involved in the production of the pigment, supporting

209 the hypothesis of its manufacture through ingestion, digestion and urination by cows. However,

210 sulphotransferase enzymes are also present in plants, and sulphonated xanthones [62] and flavonols

211 [65] have been isolated. Accordingly, the identification of this compound cannot alone validate the

212 animal-based production process described above.

213

214 **3.2 Photophysical properties**

215 The absorbance spectrum of sample NG covers the range between *c*.250 and 550 nm,

216 imparting the dark yellow colour to the powder. The bands in the UV region can be attributed to π-

217 π^* transitions, while those at longer wavelengths (> 400 nm) are of n-> π^* (S_0 > S_1) nature [39] (see

218 also the TDDFT calculations in section 3.4). The excitation spectrum, obtained by monitoring the

219 emission at 600 nm, closely matches the absorption profile, pointing to a lack of intermediate

220 photo-induced processes between absorption and emission. Both samples (NG and B64) emit in the

9

221 yellow-orange region with a maximum around 600 nm (Figure 2). The corresponding lifetime

222 decays (Figure 2, inset) are in good accordance with a bi-exponential model (B64: $\tau_1 = 510$ps

223 (73%), $\tau_2 = 1.50$ ns (27%); NG: $\tau_1 = 530$ps (75%); $\tau_2 = 1.49$ns (25%)), suggesting the presence of

224 different packed domains (driven by the π-π stacking and hydrogen bonds), which commonly occur

225 in solid-state organic samples [66]. For the first time, it was possible to measure the

226 photoluminescence quantum yield (PLQY) of a solid sample of Indian yellow: PLQY(NG) = 0.6%.

227 Unfortunately, the sub-millimetric sample from the wall panting was too small to measure its

228 PLQY. The < 10 nm hypsochromic shift between the emission maxima of the two samples can be

229 attributed to the different ratios of EA and E.

230
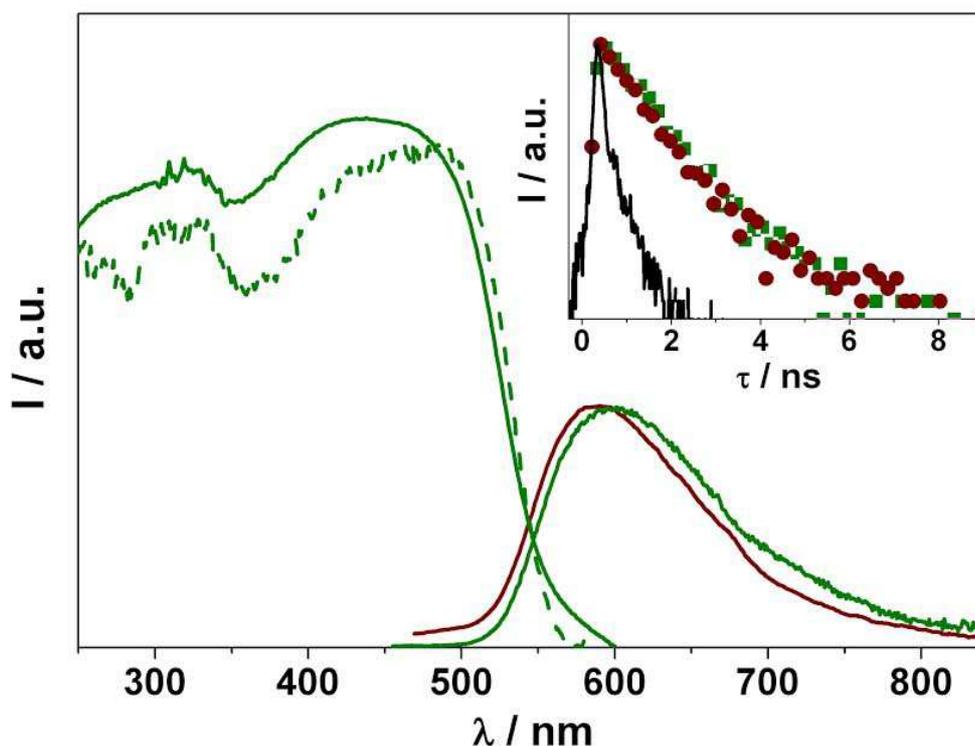
241 **Fig. 2** Absorbance (total reflection, full line), excitation (dashed line, λ_{em} = 600 nm) and normalised

242 emission (full line, λ_{exc} = 407 nm) spectra of powdered NG (dark green line) and B64 (dark red

243 line). Inset: sample luminescence decays and instrument response (black full line).

244 **3.3 Imaging**

245   Figure 3 shows the visible (top), UV-induced visible (middle) and UV-induced IR (bottom)

10

246 luminescence images of the overall area from which sample B64 was taken (as illustrated in Figure

247 1). Indian yellow is characterised by a yellow-orange fluorescence, in keeping with the emission

248 maximum at 600 nm following excitation at 407 nm revealed by PL spectroscopy. The emission of

249 Indian yellow also occurs in the IR range (*c*.700-800 nm range, Figure 2), and it can be observed in

250 the UV-induced IR imaging (*c*.700-1000 nm range) as 'glowing white', against a grey-black

251 background. Areas in the UV-induced visible image that show a paler yellow fluorescence may

252 indicate the presence of other compounds and further investigation and analysis is ongoing.

253 Because of the relatively high PLQY of Indian yellow, it was possible to image a large

254 section (c.10 m^2) of the ceiling in a single frame from a distance of about 5 m, by firing the flashes

255 many times during a 30s exposure (Figure 4).

256

257

258

259

260

261

262

263

264

265

266

267

268
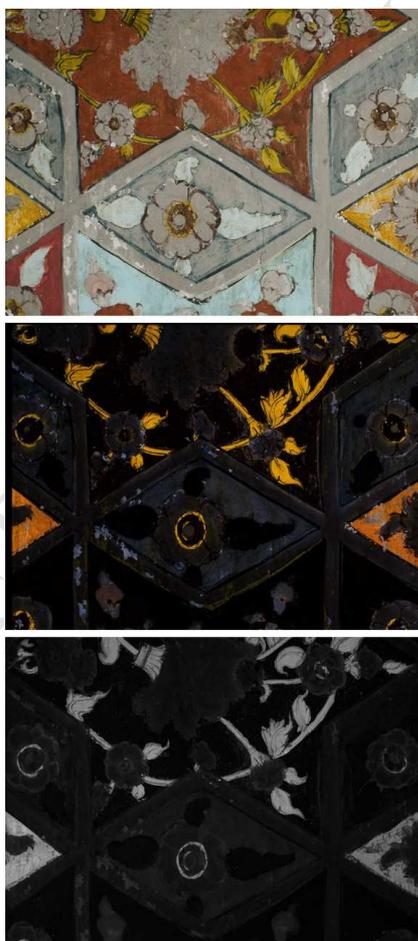
269 **Fig. 3** Area from which sample B64 was taken; visible image (top), UV-induced visible (middle)

270 and UV-induced IR (bottom) luminescence images. Indian yellow is characterised by a yellow-

271 orange fluorescence. Areas showing a paler yellow fluorescence may contain other compounds.

11
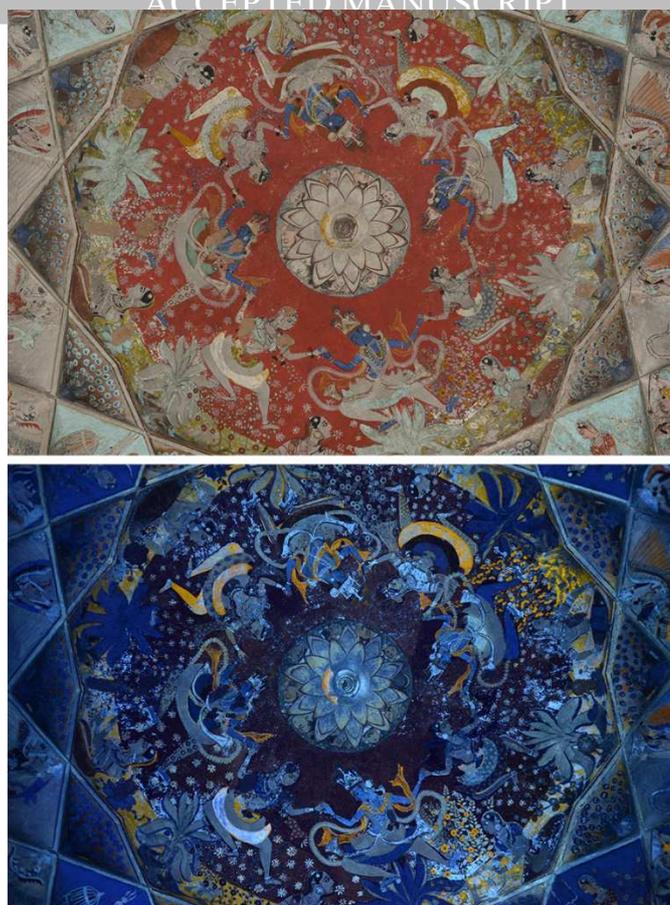
272

273

274

275

276

277

278

279

280

281 **Fig. 4** Ceiling of the Badal Mahal, Garh Palace, Bundi (Rajasthan, India) depicting Krishna dancing

282 with the *gopis*; (top) visible image and (bottom) UV-induced luminescence image, showing the

283 yellow-orange emission of Indian yellow. Due to the distance between the camera and the ceiling,

284 the use of a white board and Spectralon® reflectance standards was impossible, thus precluding

285 correction for inhomogeneous light distribution and ambient stray light.

286 **3.4 TDDFT calculations**

287   Results of benchmarks of the present study for EA, SE and E are presented in Tables S1, S2

288 and S3 in the Supplementary Material. Although pure PBE better estimates the positions of the first

289 two singlet states for all the three species with respect to the experimental reference spectrum (dark

290 green line in Figure 2), it gives a mismatch in the order of the lowest two singlet and four triplet

291 states with respect to all the other functionals investigated and previous literature data on X, which

292 found four triplet states below the optically-active S_2, where the first triplet was determined to have

293 a $^3(n_O \rightarrow \pi_L^*)$ character in a vacuum [39]. Long-range corrected hybrid functionals, known to give a

12

294   good and consistent description of low-lying excited state energies for most organics dyes [67],

295   show computed wavelengths systematically lower than those found experimentally. The B3LYP

296   functional combined with the TZVP basis set provides the best computational performance with

297   respect to the experimental excitation/absorption profile. It is, however, recognised that results

298   obtained with hybrid functionals tend to be in better agreement with experimental trends than the

299   values computed with pure functionals.

300   The lowest excited singlet state of EA, SE and E at the B3LYP/TZVP level of calculation,

301   in a vacuum, is found to be a dark $^1(n_O\pi_L^*)$ state, as for X, a chromophore well known for its

302   different solvent- and temperature-dependent photophysical properties [39-42], [68-72]. The lowest

303   state in the triplet manifold has a $^3(\pi_H-\pi_L^*)$ character, which is different to X in the gas phase [39]

304   (see Table 1): although the two lowest triplet states are energetically close in EA ($\Delta E = 0.09$ eV),

305   they are quite well separated in SE and E (0.19 eV and 0.26 eV, respectively).

306   A comprehensive comparison shown in Table 1 between the lowest triplet and singlet states

307   in a vacuum, obtained at TDDFT(B3LYP)/TZVP level of theory for: i) EA, ii) SE, iii) E, iv) OH-

308   CH_3-X and v) X, allows the identification of a bathochromic effect induced by hydroxyl groups and

309   glucuronic acid added to the benzene rings in X to form E and EA, respectively, leading to a final

310   excitation spectrum of EA moderately red-shifted with respect to X. The presence of the sulphonate

311   substituent in SE barely affects the absorption spectrum profile with respect to EA, as expected.

312   The bathochromic shift observed in the solid state optical response for both the S_1 and S_2

313   state energies, with respect to the calculated absorption wavelengths in a vacuum, can be ascribed to

314   a combined effect of intermolecular interactions (π-π stacking and hydrogen bonds) occurring

315   between packed molecules. The deprotonation of the hydroxyl group, with the resulting formation

316   of calcium and magnesium salts, could be also partially responsible for the spectral red shift.

317

318   Table 2 lists the principal TDDFT(B3LYP)/CPCM singlet vertical excitation energies (in

319   nm) calculated in water, with their electronic structure characterisation, for EA, SE and E,

320 compared with the corresponding experimental main peaks (in nm). Figure 5 shows a comparison

321 between the experimental absorption spectrum (solid black line) and theoretical stick spectra

322 obtained in water for EA (solid red lines), SE (solid green line) and E (solid blue line), scaled for

323 their relative abundance in the NG sample (see Section 3.1) and, also, with their convoluted

324 Gaussian spectrum (FWHM of 0.05 eV), as a solid thin grey line. The related frontier orbitals

325 involved in the main vertical transitions are depicted in Figures S1, S2 and S3 for EA, SE and E. As

326 shown in Table 2, the molecular orbital analysis of the DFT (B3LYP) electronic wavefunction

327 reveals, in agreement with the literature, electronic transition assignments identified for the X

328 moiety, with the order of the first two singlet states $^1(n_O \to \pi_L^*)$ and $^1(\pi_H \to \pi_L^*)$ inverted between

329 vacuum and water, due to the solvatochromic effect of the polar solvent. Indeed, in water, the

330 combined effects of polarity and hydrogen bond formation become strong enough to trigger a

331 reversal of the order of singlet states with respect to a vacuum. In our calculations, the $^1(n_O \to \pi_L^*)$

332 state experiences a blue shift of about 0.34 eV, with respect to a moderate red shift of about 0.28 eV

333 of the $^1(\pi_H \to \pi_L^*)$ state for EA. As can be easily seen in the diagram in Figure S4, this variation in

334 the energy leads to a crossing between the two singlet states. The energy blue shifts of the $^1(n_O \to \pi_L^*)$

335 $\to\pi_L^*)$ state observed in water for SE and E are 0.30 eV and 0.10 eV, respectively, while, the

336 corresponding red shifts of the $^1(\pi_H \to \pi_L^*)$ state are 0.19 eV and 0.17 eV. Moreover, the order of the

337 lowest $^3(n_O \to \pi_L^*)$ and $^3(\pi_H \to \pi_L^*)$ triplet states found in water for EA, SE and E by the

338 TDDFT(B3LYP) calculations is in agreement with the results of Rai-Constapel et al. for X in water

339 [39].

340 Our TDDFT(B3LYP) vertical excitation energies calculated on X both in the gas phase and in water

341 are in good agreement with previous theoretical and experimental data, as shown in Table 3,

342 although TDDFT predicts the lowest state in the triplet manifold with a $^3(\pi_H - \pi_L^*)$ character in

343 water, which differs from the DFT/MRCI results reported by Rai-Constapel et al. [39].

344 Furthermore, TDDFT(B3LYP) optimisations of the first two triplet states of X, $^3(\pi_H - \pi_L^*)$ and

345 $^3(n_O \pi_L^*)$, in a vacuum, provide adiabatic excitation energies of, respectively, 433 and 428 nm, in

14

346 agreement with experimental phosphorescence data in 3-methylpentane [68] or in hexane solution

347 at room temperature [69].

348

349

350

351

352

353

354

355

356

357
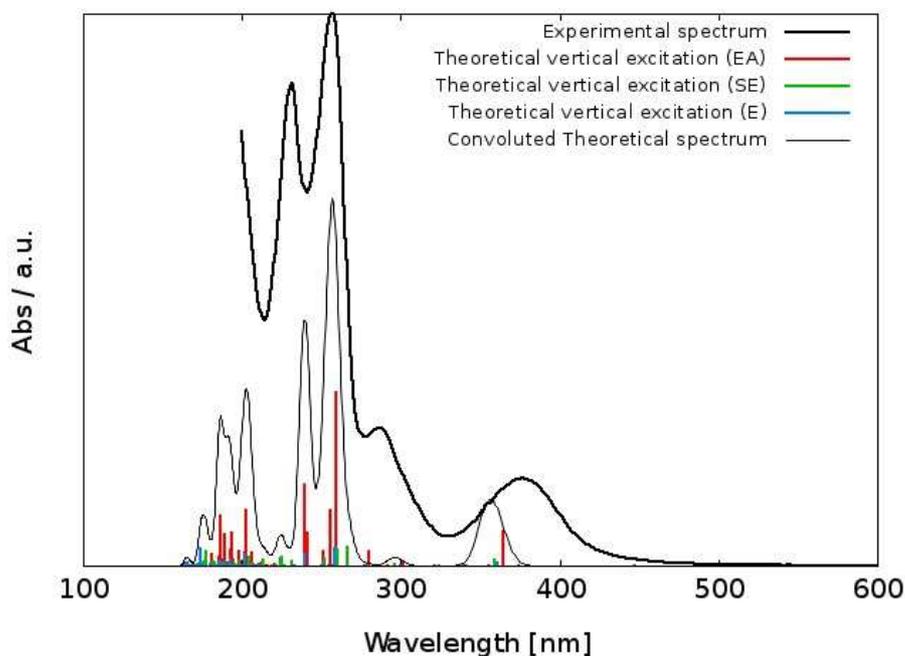
358 **Fig. 5** The experimental absorption spectrum (solid black tick line) in water of NG Indian yellow,

359 with stick theoretical TD-B3LYP/TZVP/CPCM spectra for EA (red line), SE (green line) and E

360 (blue line) calculated in water and scaled for their relative abundance in the NG sample and their

361 corresponding Gaussian convoluted theoretical spectrum, with FWHM of 0.05 eV (grey solid thin

362 line).

363

364 **Table 1.** TDDFT(B3LYP/TZVP) lowest singlet and triplet vertical excitation energies, nm, in a

365 vacuum for euxanthic acid (EA), 4-sulphonate-euxanthone (SE), euxanthone (E), 1-hydroxy-7-

366 methyl-xanthone (OH-CH$_3$-X) and xanthone (X) molecules.

State	Electronic structure	TDDFT(B3LYP/TZVP) ΔE (nm)				
		(EA)	**(SE)**	**(E)**	**(OH-CH$_3$-X)**	**(X)**
S$_0$	ground state	0	0	0	0	0
S$_1$	n$_O$ ->π_L*	352	351	349	353	341
S$_2$	π_H -> π_L*	336	340	343	348	315
T$_1$	π_H -> π_L*	412	425	431	433	394
T$_2$	n$_O$ ->π_L*	400	399	396	401	384
T$_3$	(π_{H-1}->π_L*)[a];	369	368	370	370	359

15

	$(\pi_{H-2}\text{->}\pi_L*)^b$; $(\pi_{H-3}\text{->}\pi_L*)^c$ $(\pi_{H-4}\text{->}\pi_L*)^d$				
T$_4$	$(\pi_{H-4}\text{->}\pi_L*)^e$; $(\pi_{H-2}\text{->}\pi_L*)^f$ $(\pi_{H-3}\text{->}\pi_L*)^g$	358	357	356	361	353

367   [a] E and OH-CH$_3$-X; [b] EA; [c] X; [d] SE [e] E, OH-CH$_3$-X, EA; [f] X, [g] SE

368

369   **Table 2.** TDDFT(B3LYP/TZVP)/CPCM principal singlet vertical excitation energies of euxanthic

370   acid (EA) 4-sulphonate-euxanthone (SE) and euxanthone (E), nm, in water, oscillator strengths,

371   corresponding electronic structure and experimental main peaks in water, nm.

Elect. structure	TDDFT(B3LYP/TZVP)/CPCM ΔE (nm)			Osc. Strength			Exp. maximum peaks (nm)
	EA	SE	E	EA	SE	E	
$^1(\pi_H \text{-> } \pi_L*)^{a,b,c}$	363	359	360	0.1329	0.1235	0.1260	376
$^1(n_O \text{->}\pi_L*)^{a,b,c}$	321	323	339	0.0001	0.0000	0.0000	
$^1(\pi_{H-1}\text{-> } \pi_L*)^{a,b,c}$	301	296	299	0.0156	0.0158	0.0086	
$^1(\pi_{H-2}\text{->}\pi_L*)^a$; $^1(\pi_H \text{-> } \pi_{L+1}*)^{a,b,c}$; $^1(\pi_{H-3}\text{->}\pi_L*)^{b,c}$	279	278	277	0.0564	0.0185	0.0033	287
$^1(\pi_{H-4}\text{->}\pi_L*)^a$; $^1(\pi_H \text{-> } \pi_{L+1}*)^{a,b,c}$; $^1(\pi_{H-3}\text{->}\pi_L*)^c$ $^1(\pi_{H-2} \text{-> } \pi_L*)^a$	259	266	257	0.6741	0.3956	0.6489	256
$^1(\pi_{H-4} \text{-> } \pi_L*)^a$ $^1(\pi_H \text{-> } \pi_{L+2}*)^b$	255	259		0.2157	0.3259		
$^1(\pi_{H-5} \text{-> } \pi_L*)^a$; $^1(\pi_{H-4} \text{-> } \pi_L*)^{b,c}$	251	252	251	0.0547	0.1503	0.0429	
$^1(\pi_H \text{->}\pi_{L+2}*)^{a,c}$; $^1(\pi_{H-1} \text{-> } \pi_{L+2}*)^b$	240	231	239	0.1276	0.0980	0.4190	
$^1(\pi_H \text{-> } \pi_{L+3}*)^{a,b,c}$	239	224	221	0.3156	0.1948	0.0176	230
$^1(\pi_{H-1} \text{-> } \pi_{L+1}*)^b$; $^1(\pi_{H-1} \text{-> } \pi_{L+2}*)^b$		223			0.1512		
$^1(\pi_{H-3} \text{-> } \pi_{L+1}*)^b$		213			0.1129		
$^1(\pi_H \text{-> } \pi_{L+5}*)^b$		204			0.1734		
$^1(\pi_{H-4} \text{-> } \pi_{L+1}*)^{a,c}$; $^1(\pi_{H-2} \text{-> } \pi_{L+1}*)^a$	202		206	0.2155		0.0614	
$^1(\pi_{H-4} \text{-> } \pi_{L+2}*)^b$; $^1(\pi_{H-4} \text{-> } \pi_{L+1}*)^c$		201	201		0.2342	0.3700	
$^1(\pi_{H-4} \text{-> } \pi_{L+2}*)^b$; $^1(\pi_{H-1} \text{-> } \pi_{L+3}*)^c$		201	192		0.1611	0.2090	
$^1(\pi_{H-1} \text{-> } \pi_{L+4}*)^a$	193			0.1264			
$^1(\pi_{H-5} \text{-> } \pi_{L+3}*)^a$	186			0.1924			

372   [a] electronic configuration ef EA, [b] electronic configuration of SE, [c] electronic configuration of E

373

16

374 **Table 3.** Vertical lowest singlet and triplet excitation energies, nm, from the ground state of

375 xanthone in a vacuum and in water calculated at the TDDFT(B3LYP)/CPCM level of theory with

376 TZVP basis set, compared with available theoretical (DFT/MRCI) and experimental literature data.

state	Electronic structure	TDDFT(B3LYP/TZVP) ΔE (nm)		DFT/MRCI ΔE (nm) literature [a]		Experimental literature [b],[c],[d]
		vacuum	water	vacuum	water	
S_0	ground state	0.00	0.00	0.00	0.00	
S_1	$n_O \rightarrow \pi_L^*$	341	315	360	307	371[b], 361 [c], 360 [d]
S_2	$\pi_H \rightarrow \pi_L^*$	315	331	319	337	325 [b], 339 [c], 336 [d]
T_1	$n_O \rightarrow \pi_L^*$	394	410	380	319	387 [b], 393 [c], 385 [d]
T_2	$\pi_H \rightarrow \pi_L^*$; $\pi_{H-2} \rightarrow \pi_L^*$	384	347	373	396	386 [c]
T_3	Multiconfigurational triplet state	359	359	346	348	
T_4	Multiconfigurational triplet state	353	358	338	348	

377 [a] Ref. 39; [b] Ref. 40 [c] Ref. 42 [d] Ref. 41

378

379 **CONCLUSION**

380 For the first time the optical properties of Indian yellow were determined quantitatively in the solid

381 state and correlated with its chemical composition. Although the main components of the pigment −

382 euxanthic acid and euxanthone − were known, the presence of a sulphonate derivative of

383 euxanthone ($C_{13}H_8O_7S$) was identified for the first time in both samples analysed in this study. A

384 theoretical analysis carried out on euxanthic acid, 4-sulphonate-euxanthone and euxanthone, both as

385 isolated molecules and in a polar (protic) solvent, helped assign the origin of the excited states

386 involved in the photo-induced processes and their electronic configurations. Additional calculations

387 on differently substituted xanthone molecules provide information on the role of substituents in the

388 absorption band positions. In depth characterisation of the photophysical properties of pigments

389 with PL spectroscopy and confirmation by theoretical calculations allow a more reliable

390 interpretation of PL imaging results and the selection of optimum excitation and emission

391 wavebands to differentiate pigments based on their luminescence properties. Further research on the

392 topic is ongoing and will be reported in more detail in due course. The extent to which this pigment

393 was used on a wall painting was previously unknown. The widespread occurrence of organic

394 pigments and colorants on Asian murals remains overlooked. Such materials are inherently

395 susceptible to damage during conservation interventions and when exposed to unfavourable

396 environmental conditions, including exposure to electromagnetic radiation or pollution, and

397 changes in relative humidity. Therefore, spatial information on their presence in works of art is of

398 paramount importance for the effective design, implementation and monitoring of appropriate

399 conservation management plans.

400

412

413 **REFERENCES**

414 [1] Baer NS, Joel A, Feller RL, Indictor N. Indian yellow. In: Feller RL, editor. Artists'

415 pigments: a handbook of their history and characteristics. Washington DC: National Gallery of

416 Art; 1986. p. 17-36.

417 [2] Mukharji TN. Piuri or Indian yellow. Journal of the Society of the Arts. 1883-84;32:16-7.

418 [3] Heaton N. Outlines of paint technology. London: C. Griffin & Company Limited, 1947.

419 [4] Artz NE, Osman EM. Biochemistry of glucuronic acid. New York: Academic Press, 1950.

420 [5] Nietzki R, Collin A, Richardson W. Chemistry of the organic dyestuffs. London: Gurney &

421 Jackson; 1892.

422 [6] Stenhouse J. Examination of a yellow substance from India called Puree, from which the

423 pigment called Indian Yellow is manufactured. The London, Edinburgh and Dublin

424 Philosophical Magazine and Journal of Science. 1844;25:321-5.

425 [7] Finlay V. Colour: travels through the paintbox. London: Sceptre, 2002.

426 [8] Mérimée JFL. The art of painting in oil and in fresco being a history of the various

427 processes and materials employed, from its discovery, by Hubert and John Van Eyck, to the

428 present time. London: Whittaker & Co, 1839.

429 [9] Bailkin J. Indian Yellow: Making and Breaking the Imperial Palette. J Mat Cult.

430 2005;10(2):197-214.

431 [10] Ravindran TR, Arora AK, Ramya S, Subba Rao RV, Raj B. Raman spectroscopic study of

432 medieval Indian art of 17th century. J Ram Spect. 2011;42(4):803-7.

433 [11] Reiche I, Britzke R, Bukalis G, Reinholz U, Weise HP, Gadebusch RD. An external PIXE

434 study: Mughal painting pigments. X-Ray Spect. 2005;34(1):42-5.

435 [12] Purinton N, Newman RA. Technical analysis of indian painting materials. In: Walker DS,

436 editor. Pride of the Princes: Indian art of the Mughal era in Cincinnati Art Museum: Cincinnati

437 Art Museum; 1985. p. 107-13.

438 [13] Townsend JH. The materials of J.M.W. Turner: pigments. Stud in Cons. 1993;38(4):231-

439 54.

440 [14] Ploeger R, Shugar AN. The identification of natural Indian Yellow and other historic late

441 19th century pigments from the Toulouse-Lautrec estate in France. Emergency: preparing for

442   disaters and confronting the unexpected in conservation, AIC joint 44th annual meeting and

443   42nd annual conference, May 13-17, 2016, Montreal, Canada: AIC; 2016.

444   [15] Otlowska O, liwka-Kaszynska M, lebioda M, Wachowiak M. Identification and

445   characterization of the Indian Yellow dyestuff and its degradation products in historical oil

446   paint tube by liquid chromatography mass spectrometry. RSC Adv. 2015;5(60):48786-92.

447   [16] Stonor K, Morrison R. Adolphe Monticelli: the materials and techniques of an

448   unfashionable artist. Nat Gal Tech Bul. 2012;33:50-72.

449   [17] Newman RA, Weston C, Farrell E. Analysis of watercolor pigments in a box owned by

450   Winslow Homer. JAIC. 1980;19(2):103-5.

451   [18] Beach MC. Bundi Fort : a Rajput world. Mumbai, India: Marg Publications, 2016.

452   [19] de Faria DLA, Edwards HGM, Careaga V, Walt N, Maier MS. A definitive analytical

453   spectroscopic study of Indian yellow, an ancient pigment used for dating purposes. Forensic

454   Sci Int. 2017;271:1-7.

455   [20] Janssens K, Van der Snickt G, Vanmeert F, Legrand S, Nuyts G, Alfeld M, et al. Non-

456   Invasive and Non-Destructive Examination of Artistic Pigments, Paints, and Paintings by

457   Means of X-Ray Methods. Top Curr Chem (Z) 2016;374(6):374-81.

458   [21] Mass JL, Shugar AN. Handheld XRF for art and archaeology. Leuven, Belgium: Leuven

459   University Press; 2012.

460   [22] Manfredi M, Barberis E, Rava A, Robotti E, Gosetti F, Marengo E. Portable diffuse

461   reflectance infrared Fourier transform (DRIFT) technique for the non-invasive identification of

462   canvas ground: IR spectra reference collection. Anal Methods. 2015;7(6):2313-22.

463   [23] Brunetti B, Miliani C, Rosi F, Doherty B, Monico L, Romani A, et al. Non-invasive

464   Investigations of Paintings by Portable Instrumentation: The MOLAB Experience. Top Curr

465   Chem (Z) 2016;374(1):1-35.

466   [24] Rosi F, Miliani C, Braun R, Harig R, Sali D, Brunetti BG, et al. Noninvasive analysis of

467   paintings by mid-infrared hyperspectral imaging. Angew Chem Int Ed. 2013;52(20):5258-61.

[25] Isacco E, Darrah J. The Ultraviolet-Infrared method of analysis, a scientific approach to the study of indian miniatures. Artibus Asiae. 1993;53(3/4):470-91.

[26] Singer BW, Smith R, Gardiner DJ. Non-destructive analysis of pigments in Indian miniature paintings including the novel use of a diamond-ATR-FTIR technique. In: Parisi C, Buzzanca G, Paradisi A, editors. 8th International Conference on "Non-destructive investigations and microanalysis for the diagnostics and conservation of the cultural and environmental heritage": Lecce (Italy), 15-19 May 2005. Brescia: Associazione Italiana Prove non Distruttive Monitoraggio Diagnostica; 2005.

[27] Whittaker S. Photo-induced fluorescence imaging to characterise and map organic colorants. unpublished MA thesis, Courtauld Institute of Art, Conservation of Wall Painting Department; 2013.

[28] Verri G. The spatially resolved characterisation of Egyptian blue, Han blue and Han purple by photo-induced luminescence digital imaging. Anal Bioanal Chem. 2009;394(4):1011-21.

[29] Accorsi G, Verri G, Acocella A, Zerbetto F, Lerario G, Gigli G, et al. Imaging, photophysical properties and DFT calculations of manganese blue (barium manganate(vi) sulphate) a modern pigment Chem Commun. 2014;50(97):15297-300.

[30] Daveri A, Vagnini M, Nucera F, Azzarelli M, Romani A, Clementi C. Visible-induced luminescence imaging: A user-friendly method based on a system of interchangeable and tunable LED light sources. Microchem J. 2016;125:130-41.

[31] Bellei S, Nevin A, Cesaratto A, Capogrosso V, Vezin H, Tokarski C, et al. Multianalytical Study of Historical Luminescent Lithopone for the Detection of Impurities and Trace Metal Ions. Anal Chem. 2015;87(12):6049-56.

[32] Clementi C, Rosi F, Romani A, Vivani R, Brunetti BG, Miliani C. Photoluminescence Properties of Zinc Oxide in Paints: A Study of the Effect of Self-Absorption and Passivation. Appl Spectrosc. 2012;66(10):1233-41.

494 [33] Comelli D, Nevin A, Brambilla A, Osticioli I, Valentini G, Toniolo L, et al. On the

495 discovery of an unusual luminescent pigment in Van Gogh's painting "Les bretonnes et le

496 pardon de pont Aven". Appl Phys A. 2012;106(1):25-34.

497 [34] Comelli D, Capogrosso V, Orsenigo C, Nevin A. Dual wavelength excitation for the time-

498 resolved photoluminescence imaging of painted ancient Egyptian objects. Herit Sci 2016;4(1).

499 [35] Accorsi G, Verri G, Bolognesi M, Armaroli N, Clementi C, Miliani C, et al. The

500 exceptional near-infrared luminescence properties of cuprorivaite (Egyptian blue). Chem

501 Commun. 2009(23):3392.

502 [36] Thoury M, Delaney JK, De La Rie ER, Palmer M, Morales K, Krueger J. Near-infrared

503 luminescence of cadmium pigments: In situ identification and mapping in paintings. Appl

504 Spectrosc. 2011;65(8):939-51.

505 [37] Cesaratto A, D'Andrea C, Nevin A, Valentini G, Tassone F, Alberti R, et al. Analysis of

506 cadmium-based pigments with timeresolved photoluminescence. Anal Methods.

507 2014;6(1):130-8.

508 [38] Rosi F, Grazia C, Gabrieli F, Romani A, Paolantoni M, Vivani R, et al. UV-Vis-NIR and

509 micro Raman spectroscopies for the non destructive identification of Cd1 xZnxS solid

510 solutions in cadmium yellow pigments. Microchem J. 2016;124:856-67.

511 [39] Rai-Constapel V, Mihajlo E, Marian CM. Photophysics of Xanthone: A Quantum

512 Chemical Perusal. J Phys Chem A. 2013;117:3935-44.

513 [40] Ohshima Y, Fujii T, Fujita T, Daisuke I. S_1 $^1A_2(n\pi^*)$ and S_2 $^1A_1(\pi\pi^*)$ States of Jet-Cooled

514 Xanthone. J Phys Chem A. 2003;107:8851-5.

515 [41] Onuma S, Iijima K. Structure of Xanthone. Acta Cryst. 1990;C46:1725-7.

516 [42] Cavaleri JJ, Prater K, Bowman RM. An investigation of the solvent dependence on the

517 ultrafast intersystem crossing kinetics of xanthone. Chem Phys Lett. 1996;259(5-6):495-502.

518 [43] De Mello JC, Wittmann HF, Friend RH. An Improved Experimental Determination of

519 External Photoluminescence Quantum Efficiency. Adv Mater. 1997;9(3):230-2.

520 [44] Dyer J, Verri G, Cupitt J. Multispectral imaging in reflectance and photo-induced

521 luminescence modes: a user manual (v. 1.0). The British Museum; 2013.

522 [45] Frisch MJ. Gaussian 09, Revision D.01: Gaussian, Inc., Wallingford, CT, 2009.

523 [46] Becke AD. Density-functional thermochemistry. III. The role of exact exchange. J Chem

524 Phys. 1993;98(7):5648.

525 [47] Perdew JP, Burke K, Ernzerhof M. Generalized gradient approximation made simple.

526 Phys Rev Lett. 1996;77:3865-8.

527 [48] Adamo C, Barone V. Toward reliable density functional methods without adjustable

528 parameters: The PBE0 model. J Chem Phys. 1999;110:6158-69.

529 [49] Heyd J, Scuseria GE. Efficient hybrid density functional calculations in solids: assessment

530 of the Heyd-Scuseria-Ernzerhof screened Coulomb hybrid functional. J Chem Phys.

531 2004;121(3):1187-92.

532 [50] Yanai T, Tew DP, Handy NC. A new hybrid exchange–correlation functional using the

533 Coulomb-attenuating method (CAM-B3LYP). Chem Phys Lett. 2004;393(1–3):51-7.

534 [51] Vydrov OA, Scuseria GE. Assessment of a long-range corrected hybrid functional. J

535 Chem Phys. 2006;125(23):234109-.9.

536 [52] Perdew JP, Ruzsinszky A, Tao J, Staroverov VN, Scuseria GE, Csonka GI. Prescription

537 for the design and selection of density functional approximations: More constraint satisfaction

538 with fewer fits. J Chem Phys. 2005;123(6):062201.

539 [53] Jacquemin D, Preat J, Wathelet V, André J-M, Perpète EA. Substitution effects on the

540 visible spectra of 1,4-diNHPh-9,10-anthraquinones. CPLETT Chemical Physics Letters.

541 2005;405(4):429-33.

542 [54] Jacquemin D, Preat J, Perpète EA. A TD-DFT study of the absorption spectra of fast dye

543 salts. CPLETT Chemical Physics Letters. 2005;410(4):254-9.

544 [55] Petit L, Quartarolo A, Adamo C, Russo N. Spectroscopic Properties of Porphyrin-Like

545 Photosensitizers: Insights from Theory. J Phys Chem B. 2006;110(5):2398-404.

546 [56] Quartarolo AD, Russo N, Sicilia E. Structures and Electronic Absorption Spectra of a

547 Recently Synthesised Class of Photodynamic Therapy Agents. Chem Eur J. 2006;12(26):6797-

548 803.

549 [57] Petit L, Adamo C, Russo N. Absorption Spectra of First-Row Transition Metal Complexes

550 of Bacteriochlorins: A Theoretical Analysis. J Phys Chem B. 2005;109(24):12214-21.

551 [58] Quartarolo AD, Russo N, Sicilia E, Lelj F. Absorption Spectra of the Potential

552 Photodynamic Therapy Photosensitizers Texaphyrins Complexes: A Theoretical Analysis. J

553 Chem Theory Comput 2007;3(3):860-9.

554 [59] Barone V, Cossi M. Quantum Calculation of Molecular Energies and Energy Gradients in

555 Solution by a Conductor Solvent Model. J Chem Phys A. 1998;102(11):1995-2001.

556 [60] Cossi M, Rega N, Scalmani G, Barone V. Energies, structures, and electronic properties of

557 molecules in solution with the C-PCM solvation model. J Comput Chem. 2003;24(6):669-81.

558 [61] Lide DR. CRC handbook of chemistry and physics. Boca Raton: CRC Press, 2005.

559 [62] Hong D, Yin F, Hu L-H, Lu P. Sulfonated xanthones from Hypericum sampsonii.

560 Phytochemistry. 2004;65(18):2595-8.

561 [63] Chapman E, Best MD, Hanson SR, Wong CH. Sulfotransferases: Structure, Mechanism,

562 Biological Activity, Inhibition, and Synthetic Utility. Angewandte Chemie 2004;43(27):3526-

563 48.

564 [64] Wu B, Kulkarni K, Basu S, Zhang S, Hu M. First-Pass Metabolism via UDP-

565 Glucuronosyltransferase: a Barrier to Oral Bioavailability of Phenolics. J Pharm Sci.

566 2011;100(9):3655-81.

567 [65] Varin L, Ibrahim RK. Partial Purification and Characterization of Three Flavonol-Specific

568 Sulfotransferases from Flaveria chloraefolia. Plant Physiol. 1989;90(3):977-81.

569 [66] Srivastava AK, Singh A, Mishra L. Tuning of Aggregation Enhanced Emission and Solid

570 State Emission from 1,8-Naphthalimide Derivatives: Nanoaggregates, Spectra, and DFT

571 Calculations. J Phys Chem A. 2016;120(26):4490-504.

572 [67] Jacquemin D, Perpète EA, Scuseria GE, Ciofini I, Adamo C. TD-DFT Performance for

573 the Visible Absorption Spectra of Organic Dyes: Conventional versus Long-Range Hybrids. J

574 Chem Theory Comput. 2008;4(1):123-35.

575 [68] Pownall HJ, Huber JR. Absorption and emission spectra of aromatic ketones and their

576 medium dependence. Excited states of xanthone. J Am Chem Soc. 1971;93(24):6429-36.

577 [69] Connors RE, Christian WR. Origin of the unusual triplet-state properties of xanthones. J

578 Phys Chem 1982;86(9):1524-8.

579 [70] Ley C, Morlet-Savary F, Fouassier JP, Jacques P. The spectral shape dependence of

580 xanthone triplet-triplet absorption on solvent polarity. JPPA. 2000;137(2-3):87-92.

581 [71] Heinz B, Schmidt B, Root C, Satzger H, Milota F, Fierz B, et al. On the unusual

582 fluorescence properties of xanthone in water. Phys Chem Chem Phys 2006;8(29):3432-9.

583 [72] Satzger H, Schmidt B, Root C, Zinth W, Fierz B, Krieger F, et al. Ultrafast Quenching of

584 the Xanthone Triplet by Energy Transfer: New Insight into the Intersystem Crossing

585 Kinetics. J Phys Chem A   2004;108(46):10072.

586

587

- Photophysics, imaging and theoretical study of Indian yellow, both in solid state and in aqueous solution.

- Correlation between optical properties and chemical composition.

- Identification of a sulphonate derivative of euxanthone in 17th-century Indian wall painting.